https://doi.org/10.1016/j.nanoen.2020.104516

Hierarchically Architected Polydopamine Modified $BaTiO_3$@P(VDF-TrFE) Nanocomposite Fiber Mats for Flexible Piezoelectric Nanogenerators and Self-powered Sensors

Xiaoyang Guan, Bingang Xu,* Jianliang Gong

E-mail: tcxubg@polyu.edu.hk; Tel: +852-2766 4544

† Nanotechnology Center, Institute of Textiles and Clothing, The Hong Kong Polytechnic University, Hung Hom, Kowloon, Hong Kong, P. R. China

ABSTRACT: Flexible piezoelectric nanogenerators (FPENGs) have attracted a great attention owing to their promising applications in harvesting mechanical energy and driving portable devices. To develop high-performance FPENGs, the significant relationship among material, structure and performance inspired us a rational design of FPENGs from Pdop-$BaTiO_3$@P(VDF-TrFE) nanocomposite fiber mats with a hierarchically architected microstructure. In contrast with previous approaches, the polydopamine (Pdop) modified barium titanate ($BaTiO_3$, BT) nanoparticles have been anchored onto the surface of electrospun poly(vinylidene fluoride-trifluoroethylene) P(VDF-TrFE) fibers to fabricate hierarchical micro-structured membrane in this study, which not only effectively avoids the agglomeration of nanofillers but also enhances the density of interfaces in the nanocomposites. As a result, the as-fabricated FPENGs show a significantly enhanced output of 6V and 1.5μA as compared to the PENG with only P(VDF-TrFE) membrane (1.25V and 0.6μA). Furthermore, output voltage of the new FPENGs is 40%-68% higher than that of composite membranes with nanoparticles at the interior of nanofibers. The improved output of the PENG is attributed to the high density of interfaces in the hierarchical microstructure and the corresponding enhancement of dielectric response. Then, electric performance of FPENGs was investigated in terms of force, frequency and load resistance. Finally, the FPENG was employed to efficiently detect human body movements as self-powered sensors. The hierarchical nanocomposite membrane designed in this study provides an effective approach for developing mechanical energy harvesters, wearable sensor network and self-powered devices.

Keywords: Nanogenerator; Piezoelectric; Electrospinning; Nanocomposite; Barium titanate; Poly (vinylidene fluoride-trifluoroethylene)

1. Introduction

In the past few decades, an enormous amount of research effort has been devoted to developing eco-friendly sustainable energy storage and conversion systems for combating the global problems of energy crisis, climate change and environmental pollutions caused by the consumption and rapid depletion of fossil fuels.[1-7] Particularly, numerous attempts have been afforded to explore innovative energy conversion systems such as nanogenerators to harvest energy sources in surrounding environment for driving smart portable electronics.[8-14] Piezoelectric nanogenerators (PENGs) and triboelectric nanogenerators (TENGs) exhibit excellent capability to efficiently convert different forms of mechanical energy to electric energy, including human body motion,[15-17] vehicle movements,[8, 18, 19] water flow,[20-22] air flow,[20, 23, 24] and acoustic wave etc.[25, 26] Compared with TENGs, PENGs have the advantages of lower dimension, compact structure, high sensitivity and durability, thus have attracted considerable attention as energy harvesters, sensor networks and self-powered systems.[1] However, with the development of flexible electronics in wearable devices, implantable biomedical devices and smart textiles [27-31], the commonly used piezoelectric inorganic semiconductors (e.g., ZnO, GaN and InN), and piezoelectric ceramics (e.g., $BaTiO_3$(BT) , $ZnSnO_3$, $PbZr_xTi_{1-x}O_3$, (K, Na)NbO_3 cannot meet the demand of adequate flexibility due to their intrinsic frangibility.[32]

Because of their merits of excellent flexibility, easy processing and lightweight, piezoelectric polymers such as polyvinylidene fluoride (PVDF) and their copolymers

[e.g., poly(vinylidenefluoride-co-trifluoroethylene), P(VDF-TrFE)] show promising potential in flexible and wearable applications.[33-35] PVDF and related co-polymers based PENGs have been extensively studied to improve piezoelectric output and energy conversion efficiency for practical usage.[10, 36, 37] For instance, electrospinning is an efficient technique to realize larger piezoelectric coefficient and higher energy conversion efficiency because of the combination of the mechanical stretching and electric poling.[33, 38, 39] However, the output of polymer based PENGs is limited because the polymer materials intrinsically represent relatively low polarization and inferior piezoelectricity to inorganic piezoelectric semiconductors or piezoelectric ceramics, which restricts their applications.[40] To address this drawback, nanocomposites comprising inorganic piezoelectric nanoparticles and flexible polymers have been developed for improving the piezoelectric output performance of polymeric PENGs, taking advantages of the high piezo-response of the former and the flexibility of the latter.[1, 14, 41, 42] Among the piezoelectric polymers, P(VDF-TrFE) is attractive owing to its enhanced spontaneous polarization.[43-45] For the inorganic piezoelectric nanofillers, BT nanoparticles have been used to enhance the piezoelectric property of polymers because of their high piezoelectric coefficient, lead-free and low cost.[46-48] Currently, piezoelectric nanocomposites are normally formed by inorganic nanoparticles dispersed into piezoelectric polymer matrix (as shown in Figure 1a).[8, 46, 49-52] However, this is not an ideal construction of nanocomposite for PENGs, because of the serious agglomeration of nanofillers and inevitable deterioration of flexibility and mechanical

properties caused by the mixture of inorganic nanofillers, which downgrades the durability and stability of PENGs.[44, 53, 65] Therefore, to resolve the poor dispersion of nanofillers in polymer matrix and make full use of inorganic nanoparticles, it is of great important significance to designing a new nanocomposite structure which can not only meet the high output performance requirement but also satisfy the need for good flexibility and robust mechanical properties of PENGs.

Herein, we have designed and developed a new, facile and efficient approach to prepare Pdop-BT@P(VDF-TrFE) composite membranes with a hierarchical structure for high performance FPENGs. Specifically, P(VDF-TrFE) membranes were initially prepared by electrospinning technique to build a nanofiber network for nanoparticle adsorption. Then, BT nanoparticles were functionalized with polydopamine by *in situ* polymerization route to increase the interaction and compatibility between BT nanoparticles and P(VDF-TrFE) fibers. Finally, an ultrasonic induced adsorption process was applied to fabricate Pdop-BT@P(VDF-TrFE) nanocomposite with hierarchical structures (As shown in Figure 1b). The as-prepared PENGs not only exhibited excellent flexibility, significantly enhanced piezoelectricity and durability, but also show their potential applications for scavenging biomechanical energy and monitoring human movement as self-powered wearable sensors in our daily life.

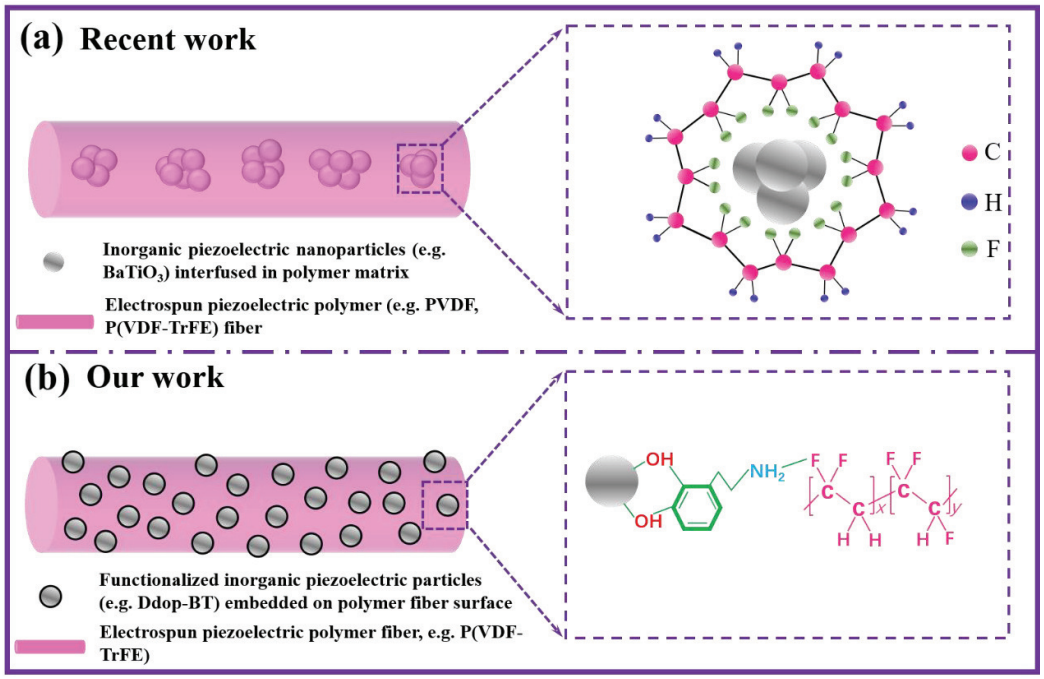

Figure 1. Schematic diagram of comparison for the different mechanisms for construction of BT/P(VDF-TrFE) nanocomposite prepared by prior art and our work. (a) BT nanoparticles showing aggregation in PVDF matrix; inset showing the β phase formation on BT nanoparticles. (b) Pdop-BT showing the good dispersion on the surface of electrospun P(VDF-TrFE) fiber; inset showing the interfacial interaction between BT, Pdop and P(VDF-TrFE).

2. Experimental

2.1 Materials

P(VDF-TrFE)-copolymer powder with a 75/25 mol % VDF/TrFE ratio was purchased from Piezotech (Piezotech S.A.S, France). Barium Titanate nanoparticles ($BaTiO_3$, cubic crystalline phase, < 100 nm particle size) was supplied by Aladdin (China), dopamine hydrochloride, Tris base, N,N-Dimethylformamide (DMF) and acetone, hydrochloric acid (HCl) purchased from Sigma-Aldrich (USA) were used as solvent for the P(VDF-TrFE). All the materials were used as received without any

further purification.

2.2 Electrospinning of P(VDF-TrFE) nanofibers

The P(VDF-TrFE) powder was dissolved in 3:7 (w/w) DMF/acetone solvent system by mechanical stirring for 8 hours at room temperature. The weight fraction of P(VDF-TrFE) in the solvent was 20 wt %. The schematic illustration of the electrospinning setup (TL-Pro, TONGLI Co. Ltd, China) is shown in Figure 2a. A 10 mL plastic syringe fitted with an 18 G stainless steel nozzle was fed by a syringe pump at a flow rate of 1 mL/h. The positive lead from a high-voltage supply was connected to the metal nozzle, and a high voltage of around 25 kV with a separation of about 14 cm between the nozzle tip and grounded electrodes was applied. The electrodes were fixed on the rotating drum with a diameter of 10 cm, which was rotated at a rate of 500 rpm, corresponding to a linear speed of 2.6 m/s at the drum surface. Figure 2b shows a digital photograph of electrospun P(VDF-TrFE) mat and the inset schematically illustrates P(VDF-TrFE) nanofiber network.

For comparison, composite nanofibers with BT or Pdop-BT nanoparticles interfused in P(VDF-TrFE) matrix were also electrospun. Prior to electrospinning, pristine BT or Pdop-BT nanoparticles were dispersed in the DMF/acetone solvent by ultrasonication for 1 h. Then, P(VDF-TrFE) was dissolved in this complex by continuous stirring for 8 h at room temperature to obtain the BT/P(VDF-TrFE) and Pdop-BT/P(VDF-TrFE) solution. The weight fractions of nanoparticles and P(VDF-TrFE) in the solvent were 4 wt% and 20 wt %, respectively. The

electrospinning is conducted under the above-mentioned conditions for 5 h.

2.3 Preparation of Pdop-BT@P(VDF-TrFE) nanocomposite mat

To prepare Pdop-BT nanoparticles decorated P(VDF-TrFE) nanofiber, 0.01 M dopamine hydrochloride and 0.2 wt% BT nanoparticles were ultrasonically dispersed in 0.01 M Tris-HCl buffer solution (pH= 8.5) and stirred for 12 hours at 60 °C, as shown in Figure 2c. After that, the resultant solution was centrifuged, dried and ground well. Finally, black colored coating was obtained over the BT nanoparticles which were white.

To prepare Pdop-BT nanoparticles anchored P(VDF-TrFE) nanofiber, different quantities of Pdop-BT nanoparticles were firstly dispersed in deionized water at various concentrations (0.05, 0.1, 0.2, 0.4, 0.6, 0.8 wt%), and then the suspensions were pre-dispersed under ultrasonication using ultrasonic processor (VCX 750, SONICS & MATERIALS. INC, USA) with a nominal frequency of 20 kHz and a power of 300 W for 1 hour (Figure 2d). Next, the loose P(VDF-TrFE) nanofiber mats (Figure 2b) were immersed into the solution for various adsorption time (1, 2, 5, 10, 20, 30 min) to determine different Pdop-BT contents in the Pdop-BT/P(VDF-TrFE) nanocomposite, where Pdop-BT nanoparticles would be gradually anchored onto the nanofiber surface under ultrasonication (Figure 2e). Therefore, the relationships between the Pdop-BT contents, output performance and adsorption time can be obtained. Pdop-BT@P(VDF-TrFE) nanocomposite mats were washed with deionized water 5 times and dried in a vacuum oven at 60 °C for 24 h. Finally, the

Pdop-BT@P(VDF-TrFE) nanocomposite was obtained (Figure 2f).

2.4 Preparation of PENGs

The power generator devices were prepared by sandwiching a Pdop-BT@P(VDF-TrFE) nanocomposite mat between two conductive fabric electrodes. Two copper wires were attached to the two electrodes separately. After cutting the sandwich structure into 2.5 cm × 2.5 cm, the whole generator device was fully packaged with polyimide tape to enhance mechanical robustness and protect it from dust and water. Finally, after the poling process (conducted on PK2674A, MEIRUIKE electronic technology co., LTD) with an electric field of 50 MV m^{-1} at room temperature for 12 h, the flexible composite based PENG was successfully fabricated.

2.5 Characterization and Measurements

Photographs were taken with a digital camera (Nikon D5600). Scanning electron microscopy images were recorded by using a TESCAN VEGA3 operating at 20 kV, and the samples were prepared by coating a thin layer of gold prior to the observation. The fiber diameter was calculated using the Image J software. The crystalline structures of the samples were determined via X-ray diffraction (Rigaku, SmartLab) and Raman spectroscopy (Nomadic Raman Microscope, BaySpec, Inc., USA). Fourier-transform infrared (FT-IR) spectra of the samples were obtained by a PerkinElmer Paragon 100 FT-IR spectrometer in the attenuated total reflectance (ATR) mode. Thermogravimetric

analysis was performed under a nitrogen atmosphere on a TGA/DSC 1-Thermogravimetric Analyzer (Mettler-Toledo International Inc.) from 100 to 800 °C with a heating rate of 10 °C/min to determine the BT content in Pdop-BT@P(VDF-TrFE) nanocomposite. The output performance of the as-prepared PENGs was evaluated by utilizing a Keyboard Life Tester (ZX-A03), which can provide a continuous dynamic sinusoidal motion with controlled levels of displacement from 0 to 10 mm and frequency from 1 to 3 Hz. The force signal was monitored by DAQ (Dewetron, Dewe-2600 DAQ system), and at the same time, the voltage signal was collected by Keysight DSO-X3014A oscilloscope and N2790A high voltage probe with 8 MΩ internal resistance. The output currents were tested using an electrometer (Keithley 6514).

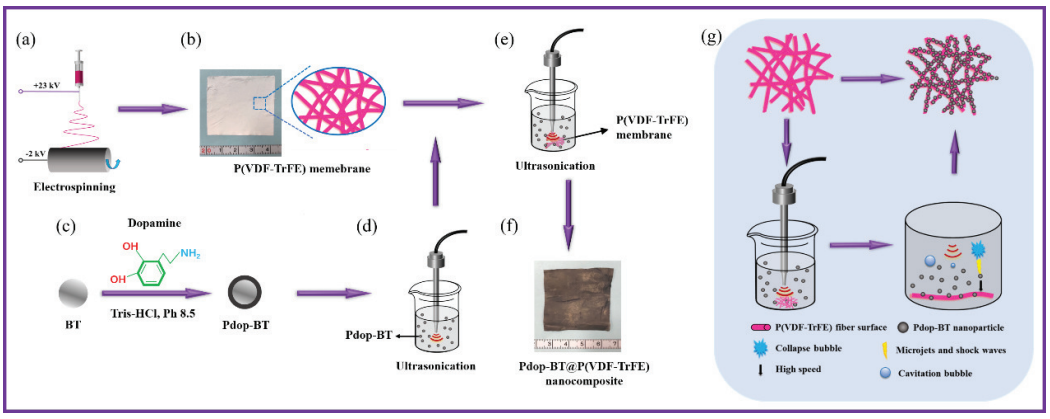

Figure 2. Schematic of preparation of Pdop-BT/P(VDF-TrFE) nanocomposite. (a) Schematic of electrospinning process; (b) A digital photograph of the as-electrospun mat (inset is illustration of P(VDF-TrFE) network); (c) schematic of preparation of Pdop-BT; (d) Preparation of Pdop-BT dispersion with ultrasonication; (e) Pdop-BT decoration using ultrasonic treatment; (f) A digital photograph of Pdop-BT@P(VDF-TrFE) nanocomposite; (g) Schematic illustration of Pdop-BT nanoparticles anchored P(VDF-TrFE) fibrous network.

3. Results and discussion

3.1 Preparation of the Pdop-BT@P(VDF-TrFE) nanocomposite

Figure 2 illustrates the fabrication of Pdop-BT@P(VDF-TrFE) nanocomposite. Firstly, P(VDF-TrFE) membranes were prepared by electrospinning technique to build a nanofiber network for nanoparticle adsorption. Secondly, The Pdop-BT nanoparticles were prepared through self-polymerization of dopamine in Tris–HCl buffer solution (pH=8.5, 10 mM) in which BT nanoparticles had already been dispersed. The as-prepared P(VDF-TrFE) nanofiber membrane was then immersed into the Pdop-BT nanoparticles suspension solution, and these nanoparticles are driven to bombard the nanofibers under ultrasonication, and finally anchored on their surfaces. The schematic demonstration of ultrasonication induced decoration of Pdop on the electrospun P(VDF-TrFE) fiber is shown in Figure 2g. Here, micro-jets and shock waves generated near the solid surfaces after collapse of the bubbles during ultrasonication can cause sintering of the nanoparticles and push Pdop-BT nanoparticles towards the nanofiber surface at very high speeds. When the fast-moving Pdop-BT nanoparticles hit the nanofiber surface, interfacial collision between Pdop-BT and P(VDF-TrFE) nanofibers occurs. Thus, the polymer nanofiber may become softened and Pdop-BT nanoparticles can be attached to the nanofiber surface.[54-56] Besides, polydopamine can work as a bridge between the BT nanoparticle and P(VDF-TrFE) fiber. The – OH group of polydopamine will attach to the surface of BT nanoparticles and at the same time the – NH group will bind to the C–F group of the P(VDF-TrFE) fiber.[47, 57-59] Hence, interaction between the BT nanoparticles and the P(VDF-TrFE) polymer will be enhanced. Figure 2b & f also show digital photographs of P(VDF-TrFE) membrane and

Pdop-BT@P(VDF-TrFE) nanocomposite. The as-electrospun P(VDF-TrFE) nanofiber mat seems loose and displays a white color. After decoration with Pdop-BT nanoparticles, it becomes dark brown.

3.2 Characterization of the Pdop-BT nanoparticles

The morphologies of the BT and Pdop-BT nanoparticles were characterized by using SEM and the typical images are shown in Fig. 3a and b, respectively. Figure 3a shows the SEM image of the as-received BT nanoparticles, which indicates that the diameter of BT nanoparticles is about 90 nm. While for the Pdop-BT nanoparticles (as shown in Figure 3b), the diameter is increased to 120.65 nm, which indicates the coating of polydopamine on the surface of BT nanoparticles and the average thickness of polydopamine is about 55 nm. The X-ray diffraction patterns of the pristine BT nanoparticles and Pdop-BT nanoparticles are shown in Figure 3c. The tetragonal phase of BT is confirmed by comparing the observed pattern with the JCPDS (# 073644) ICDD pattern. The splitting up of the peak at 45° in the XRD pattern of both BT and Pdop-BT is caused due to off-centering of Ti^{4+} ions, attributing to a tetragonal non-centrosymmetric phase in BT. The peak intensity in Pdop-BT nanoparticles is found to be slightly higher than that in the non-modified (as-received) BT nanoparticles. Raman spectra of BT and Pdop-BT are shown in Figure 3d. The spectra present peaks at 276, 305, 516 and 713 cm^{-1} suggest a tetragonal structure and the bands at 1358cm^{-1} and1568 cm^{-1} confirm the Pdop in nanocomposite.

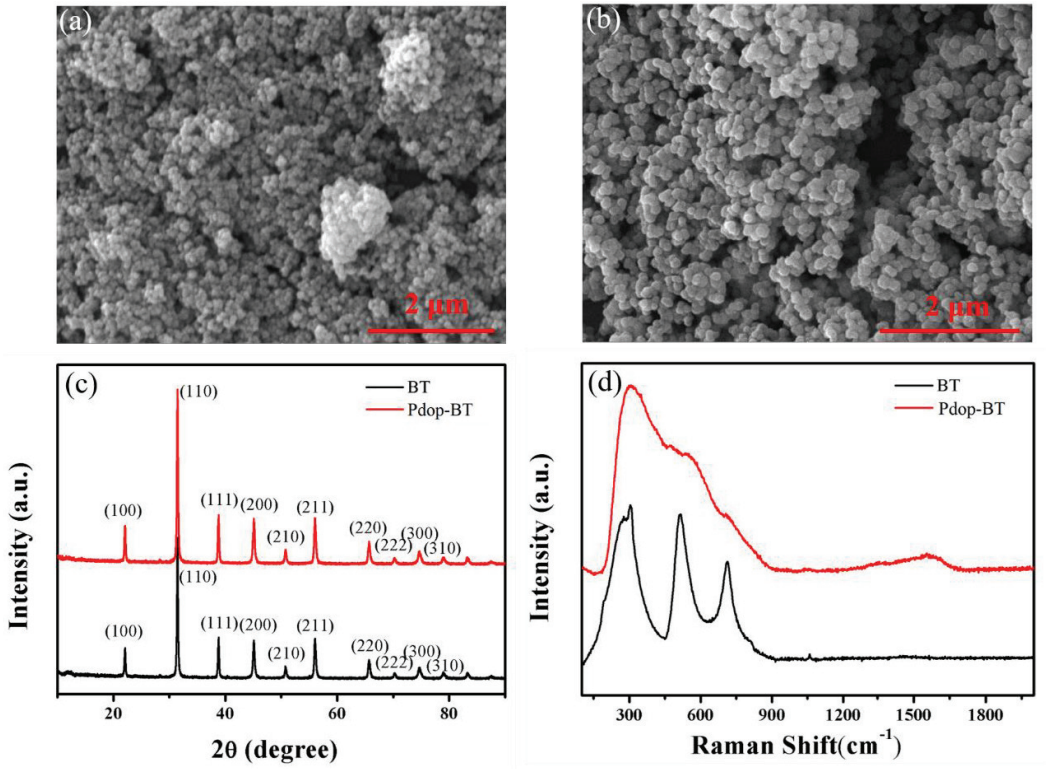

Figure 3. (a) SEM image of $BaTiO_3$ (BT) nanoparticles; (b) SEM image of dopamine functionalized $BaTiO_3$ (Pdop-BT) nanoparticles; (c) X-ray diffraction patterns of BT and Pdop-BT nanoparticles; (d) Raman spectra of BT and Pdop-BT nanoparticles.

3.3 Characterization of Pdop-BT/P(VDF-TrFE) nanocomposite

Figure 4a-b show the SEM morphology images of as-electrospun P(VDF-TrFE). The nanofibers are arranged randomly and the diameter is observed quite uniform (0.86 ± 0.19 μm). Under a higher magnification (see Figure 4b), the as-electrospun P(VDF-TrFE) nanofibers are observed to be defect free and exhibit very smooth surface with many pores and gaps among the nanofibers. Compared with the as-electrospun P(VDF-TrFE), the surface of nanofibers become very rough after the anchoring of Pdop-BT nanoparticles (see Figure 4c-d), because many Pdop-BT nanoparticles are densely adhered onto the P(VDF-TrFE) nanofiber surface. Such

interaction must be strong since Pdop-BT nanoparticles remain on the surface even after washing in deionized water for 5 times, implying that Pdop-BT nanoparticles are not simply located on the nanofiber surface. Figure 4e-f show the images of electrospun BT/P(VDF-TrFE) and Pdop/P(VDF-TrFE) composite membranes with 20 wt% BT or Pdop-BT nanoparticles (i.e. the control sample for comparison) respectively. Visible defects are easy to be found on the straight fibers, which can be ascribed to some of the incorporated BT or Pdop-BT nanoparticles aggregating and emerging from the fiber surface.[60]

Figure 4g shows the XRD pattern of the as-electrospun P(VDF-TrFE) mat and composite mat samples. The peaks of the polymer P(VDF-TrFE) are represented by 'P' and those of BT are represented by 'B'. The peak at 20.50° in the XRD pattern of the mat samples represents the reflection from (110) and (200) planes of the beta polar phase of P(VDF-TrFE). Peaks of BT are visible in the XRD pattern of nanocomposite mat containing Pdop-BT nanoparticles. The XRD pattern of the nanocomposite mat shows an additional peak at 45°, which confirms the presence of the tetragonal phase of BT in the nanocomposite.

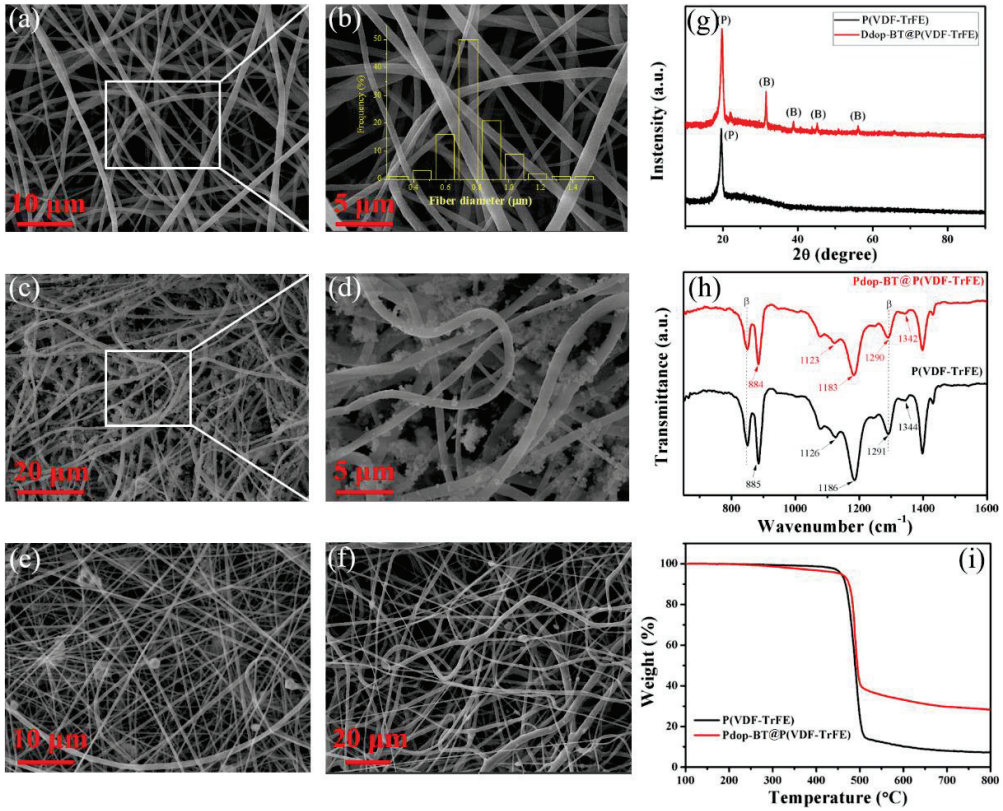

Figure 4. (a, b) The SEM images of as-electrospun P(VDF-TrFE) nanofiber membrane (inset shows the diameter distribution of nanofibers). (c, d) The SEM images of Pdop-BT@P(VDF-TrFE) nanocomposite mat. (e) The SEM image of the control sample of electrospun BT/P(VDF-TrFE) mat. (f) The SEM image of the control sample of electrospun Pdop-BT/P(VDF-TrFE) mat. (g) X-ray diffraction patterns of as-electrospun P(VDF-TrFE) and Pdop-BT@P(VDF-TrFE) nanocomposite mats. (h) The FT-IR spectra of the as-electrospun P(VDF-TrFE) and Pdop-BT@P(VDF-TrFE) nanocomposite. (i) TGA curves of as-electrospun P(VDF-TrFE) and Pdop-BT@P(VDF-TrFE) nanocomposite.

FT-IR spectroscopy was further performed on P(VDF-TrFE) and Pdop-BT@P(VDF-TrFE) to analyze the interface interaction between the Pdop-BT nanoparticles and P(VDF-TrFE) fibers. The main characteristic peaks of the samples are shown in Figure 4h. Both the as-electrospun P(VDF-TrFE) and Pdop-BT@P(VDF-TrFE) mats exhibit strong vibration peaks at 840 cm^{-1} and 1290 cm^{-1}, which are typical for the β crystalline phase. This result suggests that the

electrospinning process favors the formation of β phase crystalline. However, it can be found that several peaks for the P(VDF-TrFE) fibers have slightly shifted after the decoration of the Pdop-BT nanoparticles. For example, the peak at 1126 cm^{-1} has shifted to 1123 cm^{-1} and the peak at 1186 cm^{-1} has shifted to 1183 cm^{-1}. These changes also suggest interfacial interactions between the P(VDF-TrFE) and the Pdop-BT nanoparticles.[61-62] Specifically, the $-NH_2$ groups of dopamine may react with C-F groups of P(VDF-TrFE) based on the hydrogen bonds to form F-H bonds and such coupling interaction may induce the shift of peaks.[59] Polydopamine can be easily coated onto $BaTiO_3$ nanoparticles and modify their surface, which helps to improve the interface interactions and compatibility between $BaTiO_3$ nanoparticles and the P(VDF-TrFE) matrix.[66] The interface interactions induced by polydopamine modification may play an significant role in the formation of Pdop-BT@P(VDF-TrFE) hierarchical architecture.

TGA was also performed to evaluate the thermal stability and Pdop-BT content of the nanocomposite. As shown in Figure 4i, the Pdop-BT@P(VDF-TrFE) nanocomposite degrades in a similar manner to that of as-electrospun P(VDF-TrFE), indicating that Pdop-BT decoration would not essentially change the thermal properties of P(VDF-TrFE) nanofibers. However, the TGA curve for Pdop-BT@P(VDF-TrFE) has no obvious shift as compared to as-electrospun P(VDF-TrFE) nanofibers, indicating that the thermal stability of the P(VDF-TrFE) fibers is not obviously affected after the decoration of Pdop-BT nanoparticles. A one-step degradation process is obviously observed from the corresponding derivative thermogravimetric (DTG)

curves in Figure S1. The as-electrospun P(VDF-TrFE) begins to degrade at approximately 445 °C and the major decomposition region around 445~515 °C should be attributed to the degradation of P(VDF-TrFE) (black line in Figure S1). Compared with as-electrospun P(VDF-TrFE), the T_{max} (the temperature at which the maximum DTG occurs) of the Pdop-BT@P(VDF-TrFE) composite has no obvious shift, suggesting that the successive decoration of the Pdop-BT nanoparticles have no negative effect on the thermal stability.

The approximate content of Pdop-$BaTiO_3$ in the nanocomposite mats can be estimated using Equation 1 [61]:

$$\omega_{Pdop\text{-}BT} = C_{P(VDF\text{-}TrFE)} - C_{Pdop\text{-}BT@P(VDF\text{-}TrFE)} \quad (1)$$

where $C_{P(VDF\text{-}TrFE)}$ is the weight loss percentage of as-electrospun P(VDF-TrFE), $C_{Pdop\text{-}BT@P(VDF\text{-}TrFE)}$ is the weight loss percentage of Pdop-BT@P(VDF-TrFE) nanocomposite mat, and $\omega_{Pdop\text{-}BT}$ is the content of Pdop-BT in Pdop-BT@P(VDF-TrFE) nanocomposite mat. As can be seen in Figure 4(i), the $C_{P(VDF\text{-}TrFE)}$ and $C_{Pdop\text{-}BT@P(VDF\text{-}TrFE)}$ are about 92.17% and 71.78%, respectively. Thereby, the calculated $\omega_{Pdop\text{-}BT}$ is about 20.39%.

3.4 The basic characterization of PENG device

The digital photograph in Figure 5a shows the flexible Pdop-BT@P(VDF-TrFE) nanocomposite based PENG， which can be easily wrapped by fingers. The metal-insulator-metal framework of the all-fiber PENG is demonstrated by a three-dimensional design (Figure 5b) where flexible Pdop-BT@P(VDF-TrFE)

nanocomposite membrane (Figure 5c) was sandwiched between two flexible copper–nickel plated woven polyester conducting fabric electrodes (Figure 5d). Finally, sandwich structure was packaged with polyimide tape for protection from any environmental pollutes, such as dust and water. It is noteworthy to mention that the electric dipoles (–CH_2–/ –CF_2–) of P(VDF-TrFE) are transversely isotropic, as shown schematically in Figure 5e. The polarization direction of –CH_2/–CF_2 dipoles is perpendicular to the planar of P(VDF-TrFE) membrane due to need of low potential energy during electrospinning.[38, 63] Therefore, the maximum polarization is along thickness direction (i.e., d33 mode).

Figure 5f-h schematically described the working mechanism of Pdop-BT@P(VDF-TrFE) PENGs for generating an electrical output. This PENG device mainly works based on the piezoelectricity of electrospun P(VDF-TrFE) along with the Pdop-BT nanoparticles anchored on the surface of P(VDF-TrFE) electrospun fiber, under an external impact force. Initially, in the spatial arrangement of hydrogen and fluorine along P(VDF-TrFE) polymer chain, the difference between electron preference of atoms generates polarization in the molecules and the magnitude of polarization is proportional to the distance (r) between hydrogen and fluorine atoms. There is no piezoelectric output in the absence of external compacting force on the device because the distance (r) is unchanged (Figure 5f). When the PENG device is subject to a vertical pushing force, which makes it compressed, both the Pdop-BT nanoparticles and P(VDF-TrFE) nanofibers undergo a compressive deformation. Resultantly, with the decrease of distance (r) between hydrogen and fluorine atoms, the

polarization of P(VDF-TrFE) molecules decreases and a piezoelectric potential gradient across the nanocomposite membrane can be generated and thereby induce the formation of potential difference between the two electrodes and drive a flow of electrons between the two electrodes through the external circuit, generating a piezoelectric output current (Figure 5g). Afterwards, when the applied impact force releases, the deformation of the nanocomposite membrane recovers and the distance (r) between hydrogen and fluorine atoms increases. As a result, a reversed piezoelectric output current can be detected (Figure 5h).

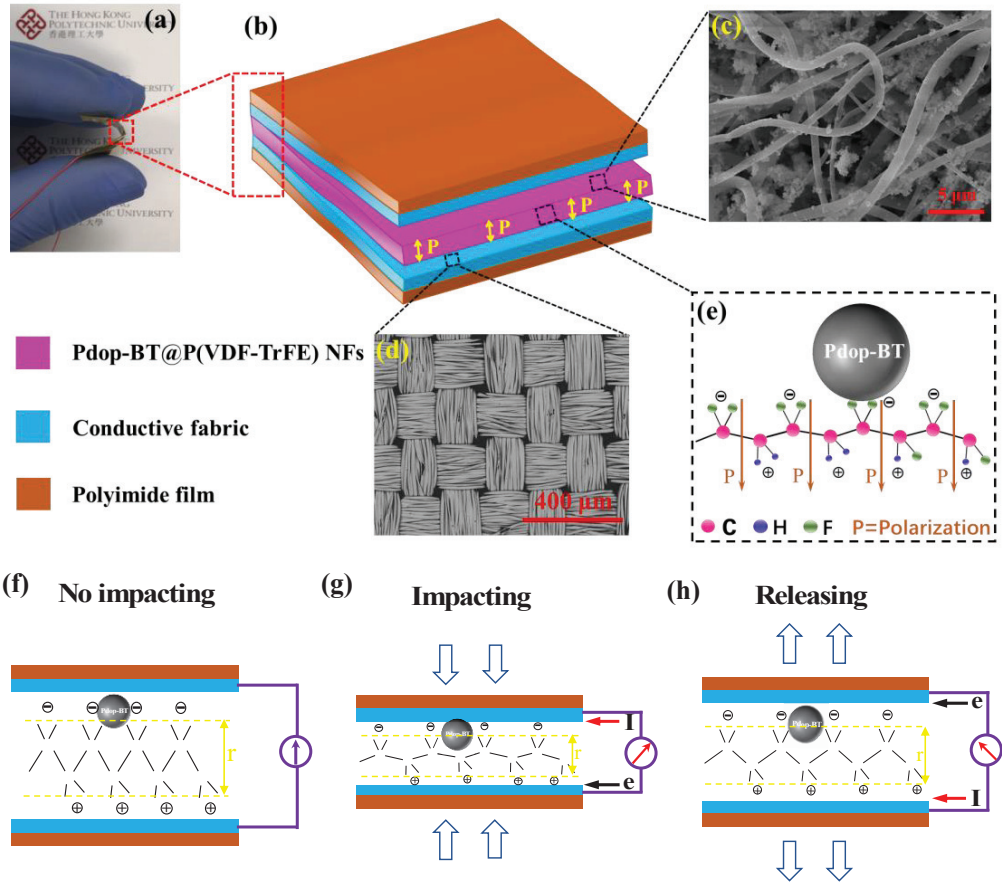

Figure 5. (a) A digital photograph of flexible Pdop-BT@P(VDF-TrFE) nanocomposite PENG. (b) Schematic illustration of the PENG structure. (c) SEM image showing the surface morphology of Pdop-BT@P(VDF-TrFE) nanocomposite membrane. (d) SEM image of Cu-Ni plated conducting fabric. (e) Schematic demonstration showing the polarization direction along the thickness direction. (f-h) Schematic diagrams showing the principles of piezoelectric output of nanocomposite based PENGs during impacting/releasing process.

3.5 Output performance characterization

The electrical output performance of the PENGs was examined on a periodic impacting/releasing machine. During the measurement, the external pushing force and frequency are maintained as constant at 700 N and 2 Hz, respectively. Firstly, the membrane thickness and output performance of electrospun P(VDF-TrFE) membrane with different spinning durations were investigated, and the representative data are shown in Figure 6a-b. As shown in Figure 6a, when the spinning time increased from 1 h to 7 h, the membrane thickness increased from 0.0054 ± 0.0013 mm to 0.0590 ± 0.0072 mm. The output voltage of electrospun P(VDF-TrFE) is observed to increase in proportional to the electrospinning duration in shorter time range (less than 5 h), meaning that the longer electrospinning time in this range can significantly improve the output voltage (shown in Figure 6b). The output voltage increases to a maximum of 0.77 V when the electrospinning time is 5 h. Unexpectedly, with further increase in the time, the output voltage decreases slightly in longer electrospinning time range. These indicate that the excessive longer electrospinning time cannot offer remarkable contribution to the improvement of output voltage, which may be attributed to the more uneven membrane thickness. Therefore, in the following section, the P(VDF-TrFE)

membrane with spinning time of 5 h will be chosen to prepare Pdop-BT@P(VDF-TrFE) nanocomposite mat.

The Pdop-BT content of Pdop-BT@P(VDF-TrFE) prepared with different concentrations of Pdop-BT suspension was carefully investigated, and the representative data are listed in Figure 6c. The Pdop-BT content is observed to generally increase with increasing the concentration of Pdop-BT suspension in lower concentration range (less than 0.4 wt %) and then increases slightly and then generally keeps constant in higher concentration range. As shown in Figure 6c, when the suspension concentration is 0.4 wt%, the Pdop-BT content of nanocomposite mat measured by weight method is about 20.4 ± 1.84 wt%, which is consistent with the amount of 20.39 wt% obtained from TGA in Figure 4i. Figure 6d show the output voltage curves of various PENG devices designed with Pdop-BT@P(VDF-TrFE) nanocomposite mats from Pdop-BT suspension of various concentrations (i.e., 0.05, 0.1, 0.2, 0.4 and 0.6 wt%). By adsorbing the Pdop-BT nanoparticles onto P(VDF-TrFE) fiber, the output performance of the resultant Pdop-BT@P(VDF-TrFE) PENG device was increased (Figure 6d), owing to the piezoelectric potential of non-centrosymmetric BT nanoparticles along with the β-phase PVDF. The output voltage values of various PENG devices increased from ~0.74 V to ~3.02 V when the concentration of Pdop-BT suspension was enhanced from 0.05 to 0.4wt% and then generally keep constant with further increase in the concentration. Therefore, the Pdop-BT@P(VDF-TrFE) nanocomposite from 0.4 wt% of Pdop-BT suspension was chosen as an optimized sample to employ in further studies. Furthermore, the influence of adsorption time of

Pdop-BT on electrical output properties was also studied. As shown in Figures 6e, the optimum adsorption time was found to be 20 min. Therefore, an adsorption time of 20 min was chosen to prepare Pdop-BT@P(VDF-TrFE) nanocomposite with high performance in the following section.

In order to affirm the superiority of our approach, electrospun BT/P(VDF-TrFE) and Pdop-BT/P(VDF-TrFE) nanocomposites with 20 wt% nanoparticles located in the interior of polymer fiber matrix were also respectively prepared for comparison, of which the mechanism is described in Figure 1a. As shown in Figure 6f, when adding BT or Pdop-BT nanoparticles into the electrospinning solutions, the electrical output voltage of the resultant electrospun fibers is increased from ~0.7 V to ~1.85 V and ~2.28 V respectively, as compared to pristine P(VDF-TrFE) electrospun mat. Such enhanced performance is consistent with the previous reported literatures and can be attributed to the enhanced piezoelectric β-phase.[40, 47, 64] However, this enhanced piezopotential is presumed to be limited by the agglomeration of BT or Pdop-BT nanoparticles in piezopolymer matrix and ineffective stress transferability.[46] Promisingly, when Pdop-BT nanoparticles were decorated on the surface of electrospun P(VDF-TrFE) fibers, the output performance of the resultant Pdop-BT@P(VDF-TrFE) device was further increased up to 3.1 V, which is 68% and 40% higher than that of BT/P(VDF-TrFE) and Pdop-BT/P(VDF-TrFE) based PENGs, respectively. The improved output of the PENG is mainly attributed to the hierarchically architected design of Pdop-BT@P(VDF-TrFE) nanocomposite mat and effective piezoelectric synergy of Pdop-BT nanoparticles and electrospun P(VDF-TrFE)

fibers. The reasons can be explained as follows: During the poling process, the existence of Pdop-BT nanoparticles, which exhibit high specific surface areas and high dielectric constant, would introduce a quantity of interface charges upon electrical field and induce localized field concentration, contributing to an enhanced efficiency in dipole polarization and the consequent piezoelectricity improvement.[67] In addition, the hierarchical structure can not only avoid the agglomeration of nanoparticles but also enhance the density of interfaces in the nanocomposites, which can reduce the defects and effectively improve the stress transfer between P(VDF-TrFE) polymer matrix and BT nanoparticles and therefore enhance the performance of PENG.

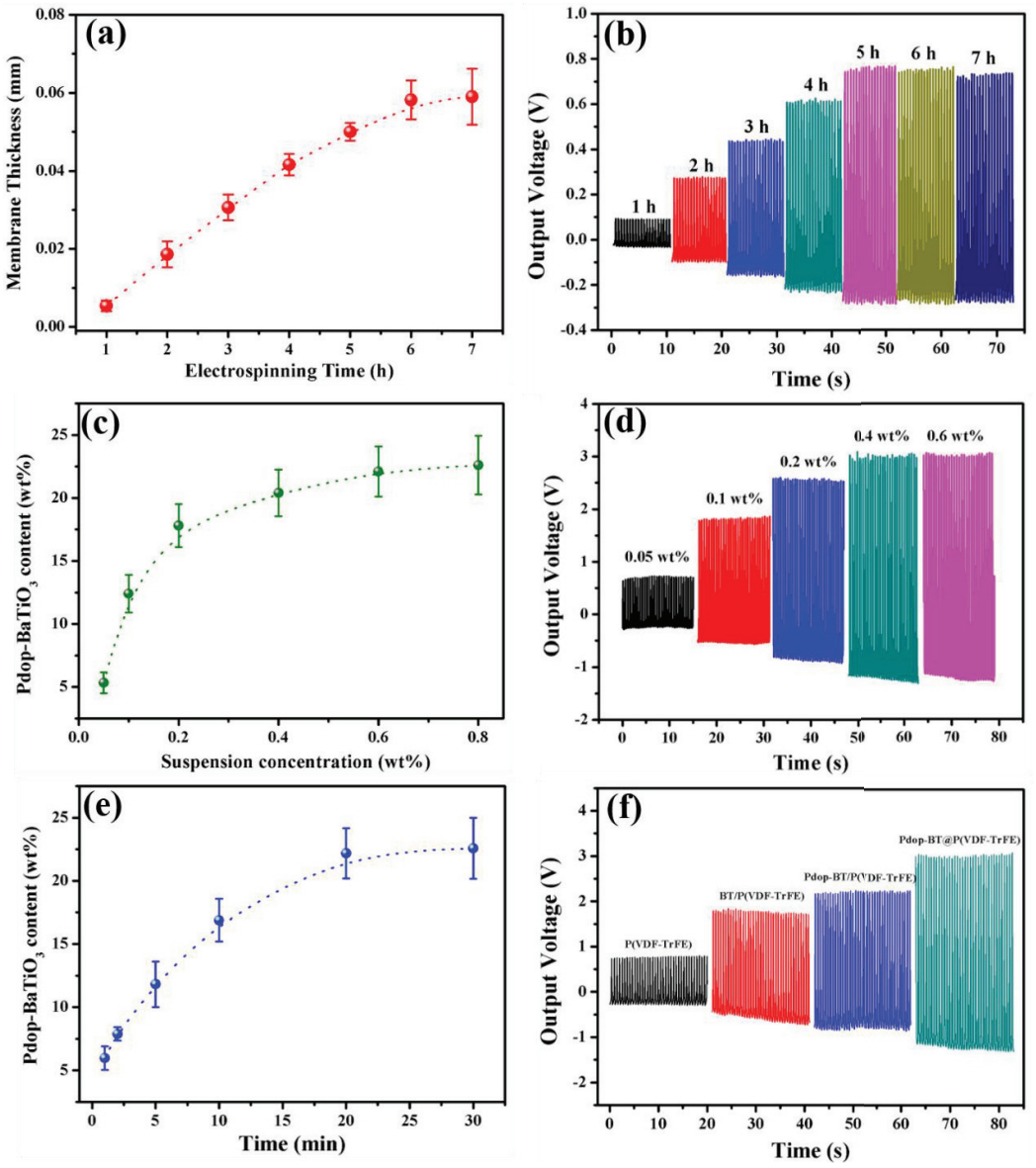

Figure 6. (a) Thickness of the P(VDF-TrFE) membranes prepared with different electrospinning times. (b) Output voltage of the P(VDF-TrFE) membranes prepared with different electrospinning times. (c) Dependence of Pdop-BT content on the concentration of suspension. (d) Output voltage curves of the Pdop-BT@P(VDF-TrFE) nanocomposite PENG from various suspension concentrations. (e) Dependence of Pdop-BT content on the adsorption time. (f) Output voltage curves of various PENGs with four composite mats of pristine P(VDF-TrFE), BT/P(VDF-TrFE), Pdop-BT/P(VDF-TrFE) and Pdop-BT@P(VDF-TrFE) under an impacting force of 700N at 2 Hz.

In the view of fact that various magnitudes of impacting forces and frequencies

could be applied to the Pdop-BT@P(VDF-TrFE) devices in the practical application scenarios, it is quite essential to evaluate the effects of external impact force and frequency on the output performance of Pdop-BT@P(VDF-TrFE) device. Figure 7a-b show the output voltages and current curves of Pdop-BT@P(VDF-TrFE) device at various impacting forces ranging from 300 to 700 N. Measured results clearly revealed that the output voltage and current values of Pdop-BT@P(VDF-TrFE) device were gradually enhanced from 1.2 V and 0.52 μA to 6 V and 1.52 μA, by enhancing the applied impacting force from 300 to 700 N, respectively. Such an enhancement is attributed to the strong electric polarization across the nanocomposite membrane of Pdop-BT@P(VDF-TrFE) PENG device at a large magnitude of applied impacting force.

To further assess the adaptability of Pdop-BT@P(VDF-TrFE) PENG to the environment, the output performance was tested under different impact frequency by maintaining the external impact force at 700 N, as shown in Figure 7c−d. The results show that both the output voltage and current of PENG increased proportionally with increasing impacting frequencies. More specifically, output voltage and current values of the device were increased from 1.8 V and 0.44 μA to 6 V and 1.52 μA, with the increase of impacting frequency from 1 Hz to 3 Hz, respectively (Figure 7c−d). This can be understood that, with the same charge transfer, a higher impacting frequency can shorten the sustained period of current peak, leading to a higher current amplitude. Such results clearly demonstrate that, along with the impacting force, the external impacting frequency can also predominantly affect the electrical output performance of

Pdop-BT@P(VDF-TrFE).

Similarly, output voltage and current of the pristine P(VDF-TrFE) based PENG show the same trend with an increase of impact magnitude and frequency, as shown in Figures S2-S3. However, as shown in Figure S3, the electrical outputs of P(VDF-TrFE) PENG are much inferior to those of Pdop-BT@P(VDF-TrFE) countparts due to the small piezoelectric coefficient of organic polymer. Specifically, the as-fabricated Pdop-BT@P(VDF-TrFE) based FPENGs show significantly enhanced electric outputs of ~6 V and ~1.5 μA, which are 4.8 times and 2.5 times over P(VDF-TrFE) based PENGs (~1.25 V and ~0.6 μA) under a pressure force of 700 N and cyclic pressing-releasing frequency of 3 Hz, as shown in Figure 7(c-d) and Figure S2(c-d). Correspondingly, the superior electrical output performance of Pdop-BT@P(VDF-TrFE) PENG demonstrates that the nanocomposite prepared in this study exhibits significantly enhanced electromechanical conversion efficiency.

The dependence of the electrical outputs on the external load resistance has been systematically studied. As shown in Figure 7e, the results show that as the external load resistance increases, the output voltage tends to increase and the output current shows the opposite trend due to the ohmic loss. The instantaneous power output calculated by $W = I^2R$ first increased and then decreased with the increase of load resistance from nearly 200 KΩ to 10 MΩ. The maximum load power density arrives at 8.78 ± 0.54 mW/m^2 with an external load resistance of 5 MΩ, as shown in Figure 7f. The load voltage and output current can reach 5.24 V and 1.05 μA, respectively. The maximum instantaneous power occurs when the external load resistance is the same as the

inherent impedance of the PENG.

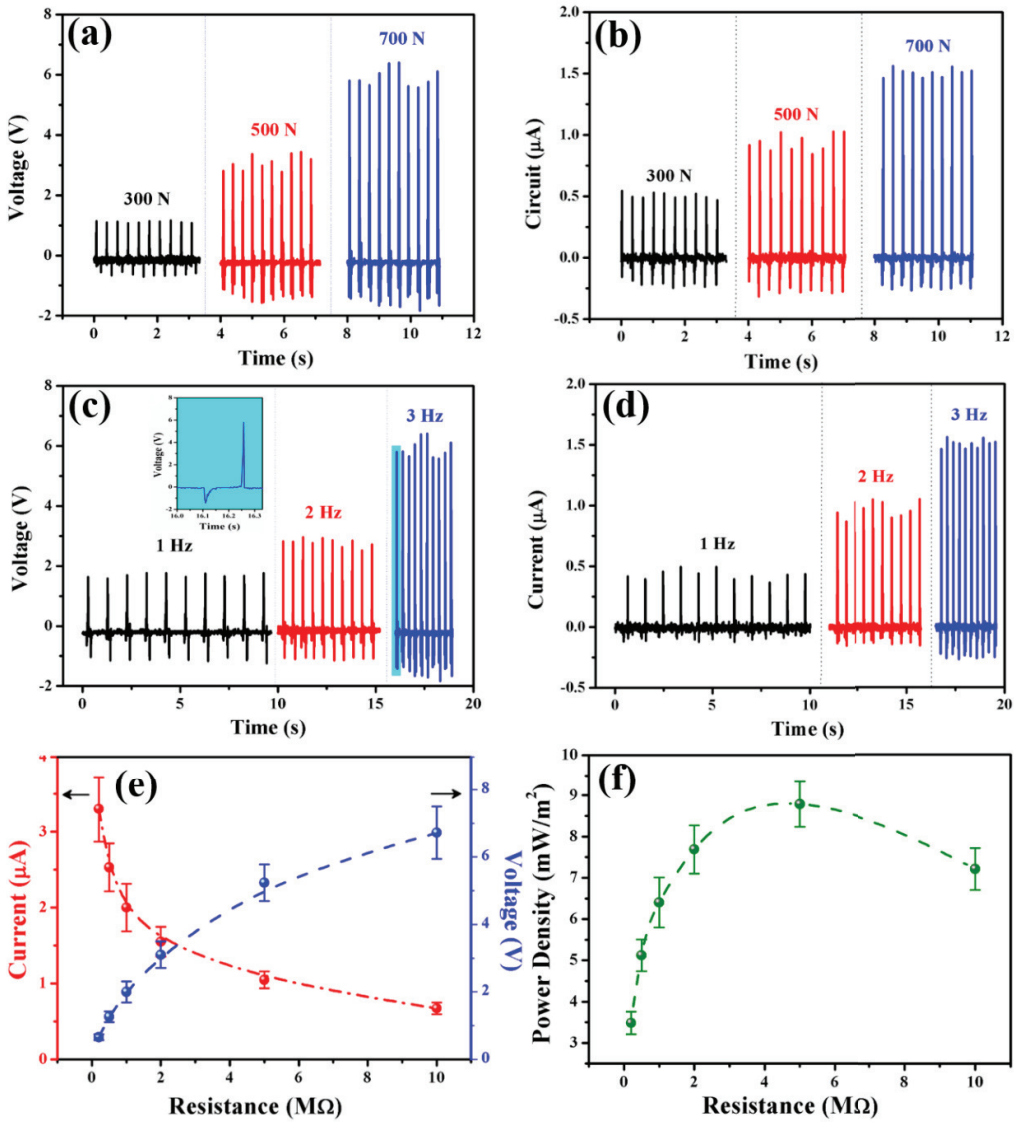

Figure 7. (a) Output voltages and (b) currents of nanocomposite based PENG at different impacting forces at a constant frequency of 3 Hz. (c) Output voltages and (d) currents of nanocomposite based PENG at different impacting frequencies under a constant pressure force of 700 N. (e) Dependence of output current and voltage on load resistance. (f) Dependence of power density on load resistance.

3.6 Application as self-powered wearable sensors

Considering the practical application in the real-life situation, it is necessary to

evaluate the stability and durability of FPENGs. As shown in Figure 8a, after 10,000 continuous impacting/releasing cycles, the electrical output performance of the Pdop-BT@P(VDF-TrFE) based FPENG can still keep stable without obvious deterioration, showing that the prepared FPENG has excellent stability and durability.

In order to explore the application potential as a useful power source, the energy-harvesting and storage capabilities of the prepared Pdop-BT@P(VDF-TrFE) nanocomposite PENG were demonstrated by charging a capacitor (C = 68 nF) using a commercial bridge rectifier circuit. Figure 8b shows the voltage-charging curve of the capacitor, which was measured under periodically impacting/releasing a PENG based on Pdop-BT@P(VDF-TrFE) nanocomposite. The bottom inset of Figure 8b shows that the rectified output power of the prepared PENG was able to effectively charge the capacitor and the voltage increased continuously with the number of impact/release cycles.

Furthermore, the Pdop-BT@P(VDF-TrFE) device is integrated into the insole of shoe to monitor human movements such as squatting up and down, walking and running. Figure 8d-f show the output voltages for squatting up and down, walking, and running when the device is fixed into the insole of a shoe (Figure 8c). The results show that the maximum output voltage for squatting up and down is about 1.78 V, which is smaller than those for walking (6.7 V) and running (7.2 V), as shown in Figure 8d–f. This is because impacting and releasing is slow and gentle during squatting up and down, whereas the frequency of running is much higher than those of walking and squatting up and down. Thus, the above results reveal that the flexible

Pdop-BT@P(VDF-TrFE) nanocomposite PENG device is potential candidate for various real-time/practical applications to harvest biomechanical energy or detect the human body movements.

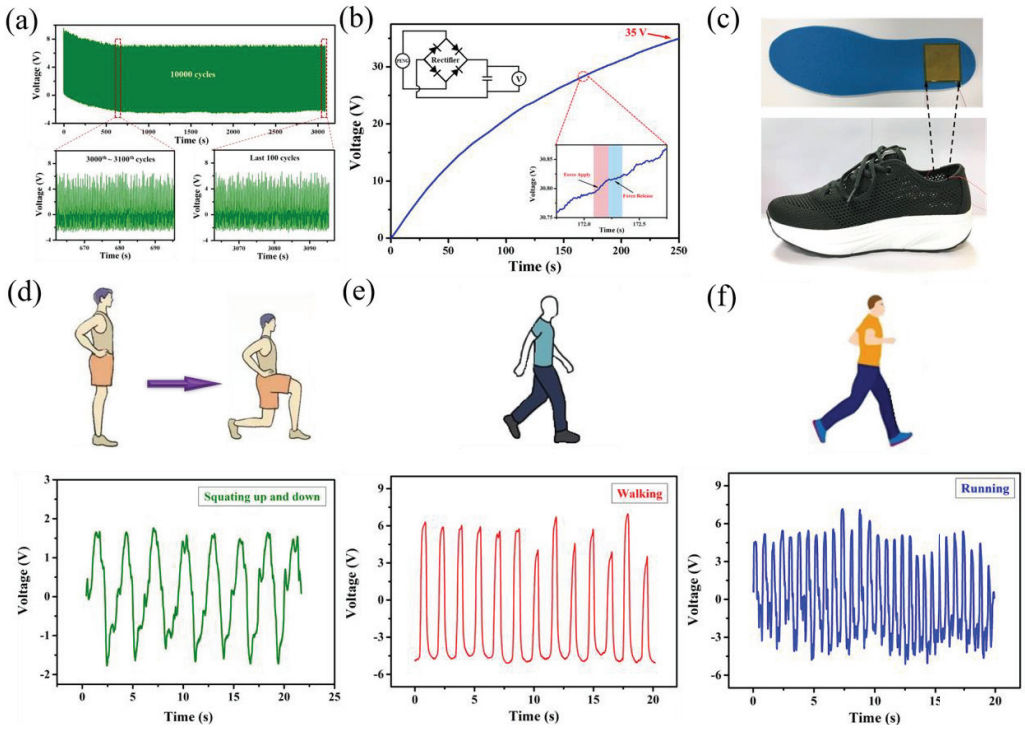

Figure 8. (a) Stability test of the Pdop-BT@P(VDF-TrFE) based PENG under 10,000 continuous working cycles (b) Voltage-charging curve of a capacitor while impacting and releasing a Pdop-BT@P(VDF-TrFE) based PENG. The top inset shows the circuit diagram and the bottom inset shows a magnified view of 3 cycles. (c) Photographs of Pdop-BT@P(VDF-TrFE) based PENG integrated into the insole of a shoe. Schematic diagrams and output voltages generated by (d) squatting up and down, (e) walking and (f) running, respectively.

To demonstrate its flexibility and potential to detect human movements, its electrical output performance under different bending conditions were systematically investigated. Figure 9a-b show the piezoelectric output voltage curves generated by the Pdop-BT@P(VDF-TrFE) PENG device at small and large bending conditions, respectively. The results reveal that the flexibility of Pdop-BT@P(VDF-TrFE) PENG

device is good enough to generate electrical outputs under various bending positions. In addition, the Pdop-BT@P(VDF-TrFE) PENG exhibited a high output voltage of ~2 V under a large bending position, while the voltage value is low (i.e., ~1 V) at the small bending position. This can be explained that the Pdop-BT nanoparticles and P(VDF-TrFE) fibers experienced a significantly increased strain under a large bending position, resulting in an enhanced output voltage. Furthermore, the Pdop-BT@P(VDF-TrFE) PENG device was put on a human hand to affirm the flexibility and detect the human hand motion. Figure 9c and insets show the output voltages and digital photographs of Pdop-BT@P(VDF-TrFE) based PENG put on a human front elbow under various elbow-bending conditions, respectively. As shown in Figure 9c, almost no output voltage signal was detected by the Pdop-BT@P(VDF-TrFE) device at the straight condition of the human arm. In contrary, the output voltage values of ~2.2 V and ~5.1 V were generated by the Pdop-BT@P(VDF-TrFE) device at the half- fold and full-fold positions of human arm, respectively. This can be attributed to the significantly high strain experienced by the Pdop-BT nanoparticles and P(VDF-TrFE) membrane under a full-fold bending condition, which results in an increased electrical output. Similarly, this PENG device can also be put on other human body parts such as fingers and utilized to detect their motions (Figure 9d). The measured results clearly affirm that the Pdop-BT@P(VDF-TrFE) device is flexible enough to generate the electrical output under various bending conditions and can be utilized to detect human movements.

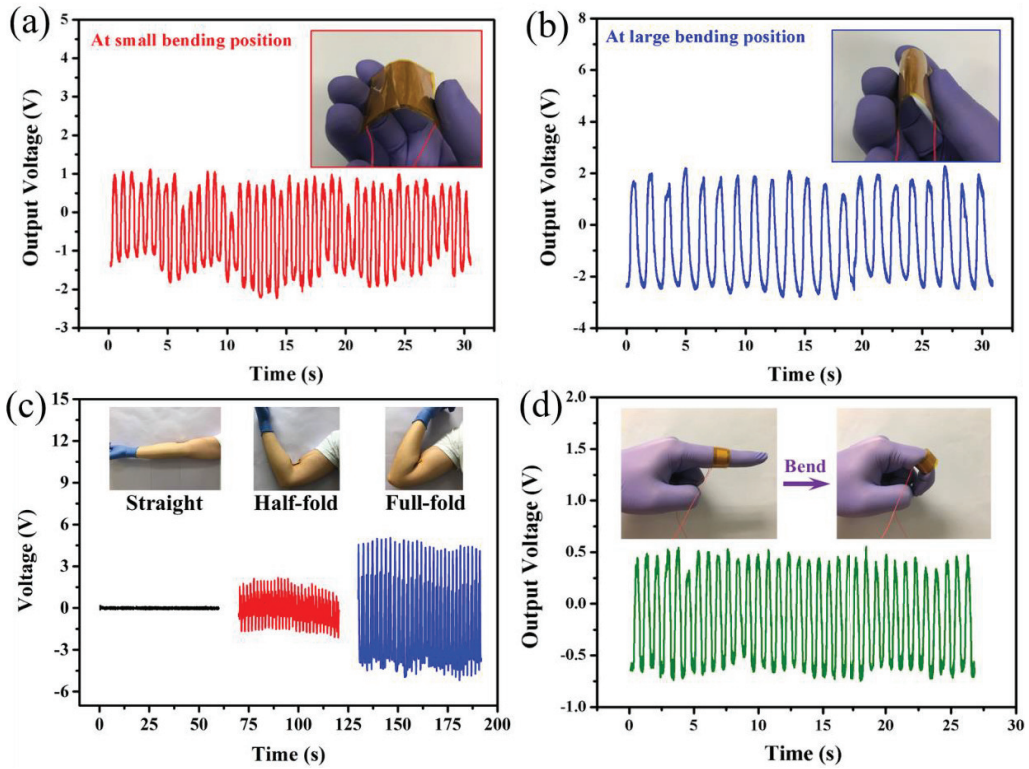

Figure 9. Demonstration for the good flexibility of the Pdop-BT@P(VDF-TrFE) PENG device. Output voltage generated by the Pdop-BT@P(VDF-TrFE) PENG at (a) small and (b) large bending positions. Insets of (a) and (b) present the photos of Pdop-BT@P(VDF-TrFE) PENG at the small and large bending positions, respectively. (c) Output voltages with elbow flexion and extension at straight, half-fold and full-fold positions, respectively. (d) Output voltages with bending index finger.

4. Conclusions

In summary, we have design and developed a hierarchically architected Pdop-BT@P(VDF-TrFE) nanocomposite via electrospinning the P(VDF-TrFE) mat and anchoring Pdop-BT@P(VDF-TrFE) on the surface of electrospun P(VDF-TrFE) nanofibers using an ultrasonication process. Herein, Pdop is employed as an effective bonder between the inorganic piezoelectric nanoparticles and polymers, displaying a new approach in the fabrication of piezoelectric nanocomposites. Resultantly, the

PENG made from Pdop-BT@P(VDF-TrFE) nanocomposite mats exhibited an obviously enhanced electric output performance in comparison with electrospun P(VDF-TrFE), BT/P(VDF-TrFE) and Pdop-BT/P(VDF-TrFE) based PENGs. Specifically, the harvested output voltage and current of Pdop-BT@P(VDF-TrFE) based PENG can reach up to ~6 V and ~1.5 μA, which are 4.8 times and 2.5 times over P(VDF-TrFE) PENG. Moreover, up to 68% and 40% of improvement in output voltage were achieved by the as fabricated Pdop-BT@P(VDF-TrFE) based PENG over BT/P(VDF-TrFE) and Pdop-BT/P(VDF-TrFE) based PENGs under the same triggering conditions, respectively. Also, it exhibited a maximum power density value of ~ 8.78 mW/m^2. Demonstration of applications showed that the nanocomposite mat based flexible PENGs can be well utilized to harvest mechanical energy and are expected to be further employed in self-powered devices.

Acknowledgment:

The authors acknowledge The Hong Kong Polytechnic University for funding supports (Project No. G-YBV2 and G-UACC) of this work. Guan Xiaoyang would also like to thank The Hong Kong Polytechnic University for providing him with a postgraduate scholarship.

References

[1] K. Shi, B. Sun, X. Huang, P. Jiang, Synergistic effect of graphene nanosheet and $BaTiO_3$ nanoparticles on performance enhancement of electrospun PVDF nanofiber mat for flexible piezoelectric nanogenerators, Nano Energy. 52 (2018) 153–162. https://doi.org/10.1016/j.nanoen.2018.07.053.

[2] Y. Chen, B. Xu, J. Xu, J. Wen, T. Hua, C.W. Kan, Graphene-based in-planar supercapacitors by a novel laser-scribing, in-situ reduction and transfer-printed method on flexible substrates, J.

Power Sources. 420 (2019) 82–87. https://doi.org/10.1016/j.jpowsour.2019.02.096.

[3] Y. Chen, B. Xu, J. Gong, J. Wen, T. Hua, C.W. Kan, J. Deng, Design of High-Performance Wearable Energy and Sensor Electronics from Fiber Materials, ACS Appl. Mater. Interfaces. 11 (2019) 2120–2129. https://doi.org/10.1021/acsami.8b16167.

[4] Y. Chen, B. Xu, J. Wen, J. Gong, T. Hua, C.W. Kan, J. Deng, Design of Novel Wearable, Stretchable, and Waterproof Cable-Type Supercapacitors Based on High-Performance Nickel Cobalt Sulfide-Coated Etching-Annealed Yarn Electrodes, Small. 14 (2018) 1–10. https://doi.org/10.1002/smll.201704373.

[5] J. Wen, B. Xu, J. Zhou, J. Xu, Y. Chen, 3D Patternable Supercapacitors from Hierarchically Architected Porous Fiber Composites for Wearable and Waterproof Energy Storage, Small. 15 (2019) 1–9. https://doi.org/10.1002/smll.201901313.

[6] J. Wen, B. Xu, J. Zhou, Y. Chen, Novel high-performance asymmetric supercapacitors based on nickel-cobalt composite and PPy for flexible and wearable energy storage, J. Power Sources. 402 (2018) 91–98. https://doi.org/10.1016/j.jpowsour.2018.09.030.

[7] J. Wen, B. Xu, J. Zhou, Toward Flexible and Wearable Embroidered Supercapacitors from Cobalt Phosphides-Decorated Conductive Fibers, Nano-Micro Lett. 11 (2019) 1–14. https://doi.org/10.1007/s40820-019-0321-x.

[8] B. Dudem, D.H. Kim, L.K. Bharat, J.S. Yu, Highly-flexible piezoelectric nanogenerators with silver nanowires and barium titanate embedded composite films for mechanical energy harvesting, Appl. Energy. 230 (2018) 865–874. https://doi.org/10.1016/j.apenergy.2018.09.009.

[9] J. Gong, B. Xu, X. Tao, Breath Figure Micromolding Approach for Regulating the Microstructures of Polymeric Films for Triboelectric Nanogenerators, ACS Appl. Mater. Interfaces. 9 (2017) 4988–4997. https://doi.org/10.1021/acsami.6b14729.

[10] J. Gong, B. Xu, X. Guan, Y. Chen, S. Li, J. Feng, Towards truly wearable energy harvesters with full structural integrity of fiber materials, Nano Energy. 58 (2019) 365–374. https://doi.org/https://doi.org/10.1016/j.nanoen.2019.01.056.

[11] Y. Jie, Q. Jiang, Y. Zhang, N. Wang, X. Cao, A structural bionic design: From electric organs to systematic triboelectric generators, Nano Energy. 27 (2016) 554–560. https://doi.org/10.1016/j.nanoen.2016.07.028.

[12] X. Cao, Y. Jie, N. Wang, Z.L. Wang, Triboelectric Nanogenerators Driven Self-Powered Electrochemical Processes for Energy and Environmental Science, Adv. Energy Mater. 6 (2016). https://doi.org/10.1002/aenm.201600665.

[13] Y. Jie, N. Wang, X. Cao, Y. Xu, T. Li, X. Zhang, Z.L. Wang, Self-Powered Triboelectric Nanosensor with Poly(tetrafluoroethylene) Nanoparticle Arrays for Dopamine Detection, ACS Nano. 9 (2015) 8376–8383. https://doi.org/10.1021/acsnano.5b03052.

[14] Y. Jie, H. Zhu, X. Cao, Y. Zhang, N. Wang, L. Zhang, Z.L. Wang, One-Piece Triboelectric Nanosensor for Self-Triggered Alarm System and Latent Fingerprint Detection, ACS Nano. 10 (2016) 10366–10372. https://doi.org/10.1021/acsnano.6b06100.

[15] R. Yang, Y. Qin, C. Li, G. Zhu, Z.L. Wang, Converting biomechanical energy into electricity by a muscle-movement- driven nanogenerator, Nano Lett. 9 (2009) 1201–1205. https://doi.org/10.1021/nl803904b.

[16] P. Bai, G. Zhu, Z.H. Lin, Q. Jing, J. Chen, G. Zhang, J. Ma, Z.L. Wang, Integrated multilayered triboelectric nanogenerator for harvesting biomechanical energy from human motions, ACS Nano. 7 (2013) 3713–3719. https://doi.org/10.1021/nn4007708.

[17] J. Zhong, Y. Zhang, Q. Zhong, Q. Hu, B. Hu, Z.L. Wang, J. Zhou, Fiber-based generator for wearable electronics and mobile medication, ACS Nano. 8 (2014) 6273–6280. https://doi.org/10.1021/nn501732z.

[18] J. Wen, B. Chen, W. Tang, T. Jiang, L. Zhu, L. Xu, J. Chen, J. Shao, K. Han, W. Ma, Z.L. Wang, Harsh-Environmental-Resistant Triboelectric Nanogenerator and Its Applications in Autodrive Safety Warning, Adv. Energy Mater. 8 (2018) 1–11. https://doi.org/10.1002/aenm.201801898.

[19] H. Askari, E. Hashemi, A. Khajepour, M.B. Khamesee, Z.L. Wang, Towards self-powered sensing using nanogenerators for automotive systems, Nano Energy. 53 (2018) 1003–1019. https://doi.org/10.1016/j.nanoen.2018.09.032.

[20] Y. Gong, Z. Yang, X. Shan, Y. Sun, T. Xie, Y. Zi, Capturing flow energy from ocean and wind, Energies. 12 (2019) 1–22. https://doi.org/10.3390/en12112184.

[21] P. Cheng, H. Guo, Z. Wen, C. Zhang, X. Yin, X. Li, D. Liu, W. Song, X. Sun, J. Wang, Z.L. Wang, Largely enhanced triboelectric nanogenerator for efficient harvesting of water wave energy by soft contacted structure, Nano Energy. 57 (2019) 432–439. https://doi.org/10.1016/j.nanoen.2018.12.054.

[22] W. Liu, L. Xu, T. Bu, H. Yang, G. Liu, W. Li, Y. Pang, C. Hu, C. Zhang, T. Cheng, Torus structured triboelectric nanogenerator array for water wave energy harvesting, Nano Energy. 58 (2019) 499–507. https://doi.org/10.1016/j.nanoen.2019.01.088.

[23] Y. Xi, H. Guo, Y. Zi, X. Li, J. Wang, J. Deng, S. Li, C. Hu, X. Cao, Z.L. Wang, Multifunctional TENG for Blue Energy Scavenging and Self-Powered Wind-Speed Sensor, Adv. Energy Mater. 7 (2017) 1–6. https://doi.org/10.1002/aenm.201602397.

[24] B. Chen, Y. Yang, Z.L. Wang, Scavenging Wind Energy by Triboelectric Nanogenerators, Adv. Energy Mater. 8 (2018) 1–13. https://doi.org/10.1002/aenm.201702649.

[25] J. Yang, J. Chen, Y. Liu, W. Yang, Y. Su, Z.L. Wang, Triboelectrification-based organic film nanogenerator for acoustic energy harvesting and self-powered active acoustic sensing, ACS Nano. 8 (2014) 2649–2657. https://doi.org/10.1021/nn4063616.

[26] F. Chen, Y. Wu, Z. Ding, X. Xia, S. Li, H. Zheng, C. Diao, G. Yue, Y. Zi, A novel triboelectric nanogenerator based on electrospun polyvinylidene fluoride nanofibers for effective acoustic energy harvesting and self-powered multifunctional sensing, Nano Energy. 56 (2019) 241–251. https://doi.org/10.1016/j.nanoen.2018.11.041.

[27] Z. Liang, B. Xu, Z. Chi, D.D. Feng, Relative Saliency Model over Multiple Images with an Application to Yarn Surface Evaluation, IEEE Trans. Cybern. 44 (2014) 1249–1258. https://doi.org/10.1109/TCYB.2013.2281618.

[28] B. Xu, L. Qu, A new practical modal method for rotor balancing, Proc. Inst. Mech. Eng. Part C J. Mech. Eng. Sci. 215 (2001) 179–190. https://doi.org/10.1243/0954406011520607.

[29] H.B. Tang, B.G. Xu, X.M. Tao, A New Analytical Solution of the Twist Wave Propagation Equation with its Application in a Modified Ring Spinning System, Text. Res. J. 80 (2010) 636–641. https://doi.org/10.1177/0040517509343817.

[30] H. Liu, X.M. Tao, K.F. Choi, B.G. Xu, Analysis of the Relaxation Modulus of Spun Yarns, Text. Res. J. 80 (2010) 403–410. https://doi.org/10.1177/0040517509342315.

[31] Z. Liang, B. Xu, Z. Chi, D. Feng, Intelligent characterization and evaluation of yarn surface appearance using saliency map analysis, wavelet transform and fuzzy ARTMAP neural network, Expert Syst. Appl. 39 (2012) 4201–4212. https://doi.org/10.1016/j.eswa.2011.09.114.

[32] D. Hu, M. Yao, Y. Fan, C. Ma, M. Fan, M. Liu, Strategies to achieve high performance

piezoelectric nanogenerators, Nano Energy. 55 (2019) 288–304. https://doi.org/10.1016/j.nanoen.2018.10.053.

[33] Y.K. Fuh, B.S. Wang, Near field sequentially electrospun three-dimensional piezoelectric fibers arrays for self-powered sensors of human gesture recognition, Nano Energy. 30 (2016) 677–683. https://doi.org/10.1016/j.nanoen.2016.10.061.

[34] C. Chang, V.H. Tran, J. Wang, Y.K. Fuh, L. Lin, Direct-write piezoelectric polymeric nanogenerator with high energy conversion efficiency, Nano Lett. 10 (2010) 726–731. https://doi.org/10.1021/nl9040719.

[35] Z. Pi, J. Zhang, C. Wen, Z. bin Zhang, D. Wu, Flexible piezoelectric nanogenerator made of poly(vinylidenefluoride-co-trifluoroethylene) (PVDF-TrFE) thin film, Nano Energy. 7 (2014) 33–41. https://doi.org/10.1016/j.nanoen.2014.04.016.

[36] Y. Mao, P. Zhao, G. McConohy, H. Yang, Y. Tong, X. Wang, Sponge-like piezoelectric polymer films for scalable and integratable nanogenerators and self-powered electronic systems, Adv. Energy Mater. 4 (2014) 1–7. https://doi.org/10.1002/aenm.201301624.

[37] C.C. Hong, S.Y. Huang, J. Shieh, S.H. Chen, Enhanced piezoelectricity of nanoimprinted sub-20 nm poly(vinylidene fluoride-trifluoroethylene) copolymer nanograss, Macromolecules. 45 (2012) 1580–1586. https://doi.org/10.1021/ma202481t.

[38] S.K. Ghosh, D. Mandal, Synergistically enhanced piezoelectric output in highly aligned 1D polymer nanofibers integrated all-fiber nanogenerator for wearable nano-tactile sensor, Nano Energy. 53 (2018) 245–257. https://doi.org/10.1016/j.nanoen.2018.08.036.

[39] J. Fang, H. Niu, H. Wang, X. Wang, T. Lin, Enhanced mechanical energy harvesting using needleless electrospun poly(vinylidene fluoride) nanofibre webs, Energy Environ. Sci. 6 (2013) 2196–2202. https://doi.org/10.1039/c3ee24230g.

[40] T. Men, X. Liu, B. Jiang, X. Long, H. Guo, Ferroelectric β-crystalline phase formation and property enhancement in polydopamine modified $BaTiO_3$/poly (vinylidene fluoride-trifluoroethylene) nanocomposite films, Thin Solid Films. 669 (2019) 579–587. https://doi.org/10.1016/j.tsf.2018.11.051.

[41] J.M. Yun, J.H. Shin, J. Ryu, N.M. Shinde, K.H. Kim, Piezoelectric Performance of Cubic-Phase $BaTiO_3$ Nanoparticles Vertically Aligned via Electric Field , Adv. Sustain. Syst. 2 (2018) 1700133. https://doi.org/10.1002/adsu.201700133.

[42] Y. Zhao, Q. Liao, G. Zhang, Z. Zhang, Q. Liang, X. Liao, Y. Zhang, High output piezoelectric nanocomposite generators composed of oriented $BaTiO_3$ NPs at PVDF, Nano Energy. 11 (2015) 719–727. https://doi.org/10.1016/j.nanoen.2014.11.061.

[43] S. Ma, T. Ye, T. Zhang, Z. Wang, K. Li, M. Chen, J. Zhang, Z. Wang, S. Ramakrishna, L. Wei, Highly Oriented Electrospun P(VDF-TrFE) Fibers via Mechanical Stretching for Wearable Motion Sensing, Adv. Mater. Technol. 3 (2018) 1–7. https://doi.org/10.1002/admt.201800033.

[44] N. Jia, Q. Xing, G. Xia, J. Sun, R. Song, W. Huang, Enhanced β-crystalline phase in poly(vinylidene fluoride) films by polydopamine-coated BaTiO3 nanoparticles, Mater. Lett. 139 (2015) 212–215. https://doi.org/10.1016/j.matlet.2014.10.069.

[45] V. Bhavanasi, V. Kumar, K. Parida, J. Wang, P.S. Lee, Enhanced Piezoelectric Energy Harvesting Performance of Flexible PVDF-TrFE Bilayer Films with Graphene Oxide, ACS Appl. Mater. Interfaces. 8 (2016) 521–529. https://doi.org/10.1021/acsami.5b09502.

[46] C.K. Jeong, C. Baek, A.I. Kingon, K. Il Park, S.H. Kim, Lead-Free Perovskite Nanowire-Employed Piezopolymer for Highly Efficient Flexible Nanocomposite Energy

Harvester, Small. 14 (2018) 1–8. https://doi.org/10.1002/smll.201704022.

[47] A. Mayeen, M.S. Kala, M.S. Jayalakshmy, S. Thomas, D. Rouxel, J. Philip, R.N. Bhowmik, N. Kalarikkal, Dopamine functionalization of $BaTiO_3$: An effective strategy for the enhancement of electrical, magnetoelectric and thermal properties of $BaTiO_3$-PVDF-TrFE nanocomposites, Dalt. Trans. 47 (2018) 2039–2051. https://doi.org/10.1039/c7dt03389c.

[48] X. Chen, K. Parida, J. Wang, J. Xiong, M.F. Lin, J. Shao, P.S. Lee, A Stretchable and Transparent Nanocomposite Nanogenerator for Self-Powered Physiological Monitoring, ACS Appl. Mater. Interfaces. 9 (2017) 42200–42209. https://doi.org/10.1021/acsami.7b13767.

[49] J. González-Benito, D. Olmos, J.M. Martínez-Tarifa, G. González-Gaitano, F.A. Sánchez, PVDF/$BaTiO_3$ /carbon nanotubes ternary nanocomposites prepared by ball milling: Piezo and dielectric responses, J. Appl. Polym. Sci. 136 (2019) 1–14. https://doi.org/10.1002/app.47788.

[50] X. Xie, C. Yang, X. dong Qi, J. hui Yang, Z. wan Zhou, Y. Wang, Constructing polymeric interlayer with dual effects toward high dielectric constant and low dielectric loss, Chem. Eng. J. 366 (2019) 378–389. https://doi.org/10.1016/j.cej.2019.02.106.

[51] Y. Wu, J. Qu, W.A. Daoud, L. Wang, T. Qi, Flexible composite-nanofiber based piezo-triboelectric nanogenerators for wearable electronics, J. Mater. Chem. A. 7 (2019) 13347–13355. https://doi.org/10.1039/c9ta02345c.

[52] K.H. Koh, Q. Shi, S. Cao, D. Ma, H.Y. Tan, Z. Guo, C. Lee, A self-powered 3D activity inertial sensor using hybrid sensing mechanisms, Nano Energy. 56 (2019) 651–661. https://doi.org/10.1016/j.nanoen.2018.11.075.

[53] D. Dhakras, S. Ogale, High-Performance Organic–Inorganic Hybrid Piezo-Nanogenerator via Interface Enhanced Polarization Effects for Self-Powered Electronic Systems, Adv. Mater. Interfaces. 3 (2016) 1–9. https://doi.org/10.1002/admi.201600492.

[54] Y. Wang, J. Hao, Z. Huang, G. Zheng, K. Dai, C. Liu, C. Shen, Flexible electrically resistive-type strain sensors based on reduced graphene oxide-decorated electrospun polymer fibrous mats for human motion monitoring, Carbon N. Y. 126 (2018) 360–371. https://doi.org/10.1016/j.carbon.2017.10.034.

[55] H. Shi, D. Shi, L. Yin, Z. Yang, S. Luan, J. Gao, J. Zha, J. Yin, R.K.Y. Li, Ultrasonication assisted preparation of carbonaceous nanoparticles modified polyurethane foam with good conductivity and high oil absorption properties, Nanoscale. 6 (2014) 13748–13753. https://doi.org/10.1039/c4nr04360j.

[56] J. Gao, M. Hu, Y. Dong, R.K.Y. Li, Graphite-nanoplatelet-decorated polymer nanofiber with improved thermal, electrical, and mechanical properties, ACS Appl. Mater. Interfaces. 5 (2013) 7758–7764. https://doi.org/10.1021/am401420k.

[57] Prateek, V.K. Thakur, R.K. Gupta, Recent Progress on Ferroelectric Polymer-Based Nanocomposites for High Energy Density Capacitors: Synthesis, Dielectric Properties, and Future Aspects, Chem. Rev. 116 (2016) 4260–4317. https://doi.org/10.1021/acs.chemrev.5b00495.

[58] M.F. Lin, V.K. Thakur, E.J. Tan, P.S. Lee, Surface functionalization of $BaTiO_3$ nanoparticles and improved electrical properties of $BaTiO_3$/polyvinylidene fluoride composite, RSC Adv. 1 (2011) 576–578. https://doi.org/10.1039/c1ra00210d.

[59] Y. Xie, Y. Yu, Y. Feng, W. Jiang, Z. Zhang, Fabrication of stretchable nanocomposites with high energy density and low loss from cross-linked PVDF filled with poly(dopamine) encapsulated $BaTiO_3$, ACS Appl. Mater. Interfaces. 9 (2017) 2995–3005.

https://doi.org/10.1021/acsami.6b14166.

[60] C. Mota, M. Labardi, L. Trombi, L. Astolfi, M. D'Acunto, D. Puppi, G. Gallone, F. Chiellini, S. Berrettini, L. Bruschini, S. Danti, Design, fabrication and characterization of composite piezoelectric ultrafine fibers for cochlear stimulation, Mater. Des. 122 (2017) 206–219. https://doi.org/10.1016/j.matdes.2017.03.013.

[61] X. Guan, G. Zheng, K. Dai, C. Liu, X. Yan, C. Shen, Z. Guo, Carbon Nanotubes-Adsorbed Electrospun PA66 Nanofiber Bundles with Improved Conductivity and Robust Flexibility, ACS Appl. Mater. Interfaces. 8 (2016) 14150–14159. https://doi.org/10.1021/acsami.6b02888.

[62] J. Gao, W. Li, H. Shi, M. Hu, R.K.Y. Li, Preparation, morphology, and mechanical properties of carbon nanotube anchored polymer nanofiber composite, Compos. Sci. Technol. 92 (2014) 95–102. https://doi.org/10.1016/j.compscitech.2013.12.008.

[63] L. Persano, C. Dagdeviren, Y. Su, Y. Zhang, S. Girardo, D. Pisignano, Y. Huang, J.A. Rogers, High performance piezoelectric devices based on aligned arrays of nanofibers of poly(vinylidenefluoride-co-trifluoroethylene), Nat. Commun. 4 (2013) 1610–1633. https://doi.org/10.1038/ncomms2639.

[64] X. Gong, Y. Chen, C.Y. Tang, W.C. Law, L. Chen, C. Wu, T. Hu, G.C.P. Tsui, Crystallinity and morphology of barium titanate filled poly(vinylidene fluoride) nanocomposites, J. Appl. Polym. Sci. 135 (2018) 2–9. https://doi.org/10.1002/app.46877.

[65] R.A. Surmenev, T. Orlova, R. V. Chernozem, A.A. Ivanova, A. Bartasyte, S. Mathur, M.A. Surmeneva, Hybrid lead-free polymer-based nanocomposites with improved piezoelectric response for biomedical energy-harvesting applications: A review, Nano Energy. 62 (2019) 475–506. https://doi.org/10.1016/j.nanoen.2019.04.090.

[66] Y. Song, Y. Shen, H. Liu, Y. Lin, M. Li, C.W. Nan, Improving the dielectric constants and breakdown strength of polymer composites: Effects of the shape of the $BaTiO_3$ nanoinclusions, surface modification and polymer matrix, J. Mater. Chem. 22 (2012) 16491–16498. https://doi.org/10.1039/c2jm32579a.

[67] L. Yang, Q. Zhao, Y. Hou, L. Hong, H. Ji, L. Xu, K. Zhu, M. Shen, H. Huang, H. He, J. Qiu, Flexible polyvinylidene fluoride based nanocomposites with high and stable piezoelectric performance over a wide temperature range utilizing the strong multi-interface effect, Compos. Sci. Technol. 174 (2019) 33–41. https://doi.org/10.1016/j.compscitech.2019.02.014.